

Projecting the Kondo Effect: Theory of the Quantum Mirage

Oded Agam and Avraham Schiller

Racah Institute of Physics, The Hebrew University, Jerusalem 91904, Israel

A microscopic theory is developed for the projection (quantum mirage) of the Kondo resonance from one focus of an elliptic quantum corral to the other focus. The quantum mirage is shown to be independent of the size and the shape of the ellipse, and experiences $\lambda_F/4$ oscillations (λ_F is the surface-band Fermi wavelength) with an increasing semimajor axis length. We predict an oscillatory behavior of the mirage as a function of a weak magnetic field applied perpendicular to the sample.

PACS numbers: 72.15.Qm, 61.16.Ch, 72.10.Fk

In a recent experiment, Manoharan *et al.* [1] used an elliptic quantum corral to project the image of a Kondo resonance over a distance of tens of angstroms, from one focus of the ellipse to the other focus. By placing a magnetic Co atom at one focus of the ellipse and measuring the tunneling current to a close-by scanning tunneling microscope (STM) tip, a distinctive Kondo resonance was seen in the I - V curve when the tip was brought directly above the Co adatom. Remarkably, a similar Kondo signature was observed when the tip was placed above the empty focus, indicating coherent refocusing of the spectral image by the surrounding corral. This should be contrasted with STM measurements of isolated magnetic adatoms on open surfaces [2,3], where a limited spatial extent of $\sim 10\text{\AA}$ was observed for the Kondo effect.

Semiclassically, one can attribute this refocusing phenomena to the property that all classical paths leaving one focus of the ellipse bounce specularly off the perimeter and converge onto the second focus with the same acquired phase [1] (see Fig. 1). However, this simple picture does not explain the quantitative features of the experiment. For example, the complex interference patterns in the dI/dV difference map throughout the ellipse, or the $\lambda_F/4$ oscillations of the mirage with an increasing semimajor axis length a (λ_F is the Fermi wavelength). Explanation of these features requires a quantitative theory, which is the objective of the present Letter.

Starting with a microscopic picture of Kondo scattering off the Co adatoms we obtain good qualitative and quantitative agreement with the experiment. We establish a remarkable feature of the quantum mirage which, aside from the $\lambda_F/4$ oscillations mentioned above, is independent of the size and the shape of the ellipse, provided the ellipses is not too small. In particular, there is no dependence on the ellipse eccentricity \mathcal{E} , see Fig. 1. In the presence of a weak perpendicular magnetic field, we predict an oscillatory behavior of the quantum mirage as a function of the magnetic flux encircled by the ellipse.

The Cu(111) surface has a band of surface states, which acts as a two-dimensional electron gas. The surface band starts 450meV below the Fermi energy, and has a Fermi wave number of $k_F^{-1} \simeq 4.75\text{\AA}$. When a Co adatom is placed on the surface, it scatters both the sur-

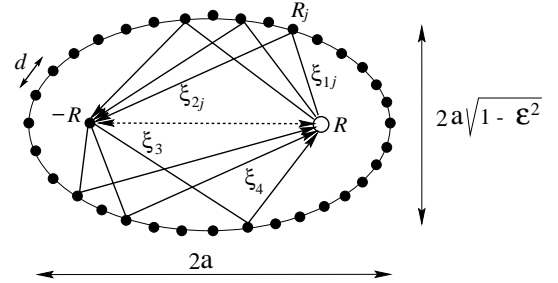


FIG. 1. An illustration of an elliptic quantum corral and the classical trajectories associated with the quantum mirage. The ellipse is characterized by a semimajor axis length a and an eccentricity \mathcal{E} . The mean distance between adjacent atoms forming the ellipse perimeter is d .

face electrons and the underlying bulk electrons. As recently shown by Újsághy *et al.* [4] for Co on Au(111), one may model the Co adatom by an effective nondegenerate Anderson impurity [5], characterized by an effective energy level ϵ_d , an on-site repulsion U , and two hybridization matrix elements t_s and t_b to the underlying surface and bulk conduction electrons. In this manner, each of the Co atoms forming the ellipse in the experiment of Manoharan *et al.* [1] acts as an Anderson impurity, as does the adatom placed inside the ellipse.

Denoting the creation of a surface-state and a bulk conduction electron by $c_{\vec{k}\sigma}^\dagger$ and $a_{\vec{q}\sigma}^\dagger$, respectively (here \vec{k} labels a two-dimensional surface vector while \vec{q} is a three-dimensional vector), we model the system by the Hamiltonian $\mathcal{H} = \mathcal{H}_{\text{surf}} + \mathcal{H}_{\text{bulk}} + \sum_{i=0}^N \mathcal{H}_{\text{imp}}(\vec{R}_i)$, where

$$\mathcal{H}_{\text{surf}} = \sum_{\vec{k}\sigma} \epsilon_{\vec{k}} c_{\vec{k}\sigma}^\dagger c_{\vec{k}\sigma} \quad \text{and} \quad \mathcal{H}_{\text{bulk}} = \sum_{\vec{q}\sigma} E_{\vec{q}} a_{\vec{q}\sigma}^\dagger a_{\vec{q}\sigma}$$

describe the free surface and bulk conduction bands, respectively, and

$$\begin{aligned} \mathcal{H}_{\text{imp}}(\vec{R}_i) = & \epsilon_d \sum_{\sigma} d_{i\sigma}^\dagger d_{i\sigma} + U d_{i\uparrow}^\dagger d_{i\uparrow} d_{i\downarrow}^\dagger d_{i\downarrow} \\ & + \sum_{\sigma} \left\{ t_s d_{i\sigma}^\dagger \psi_{\sigma}(\vec{R}_i) + t_b d_{i\sigma}^\dagger \chi_{\sigma}(\vec{R}_i) + \text{h.c.} \right\} \end{aligned}$$

describes a Co adatom at point \vec{R}_i on the surface. Here

$d_{i\sigma}^\dagger$ creates a localized Co electron at site \vec{R}_i ($i = 0$ for the inner adatom and $i = 1, \dots, N$ for the perimeter adatoms), while $\psi_\sigma(\vec{R}_i)$ and $\chi_\sigma(\vec{R}_i)$ annihilate, respectively, a surface and a bulk conduction electron at site \vec{R}_i . For simplicity, we have taken the different adatoms to be identical, and neglected any momentum dependence of t_s and t_b . In what follows, we shall mainly be interested in the case where the inner adatom is located at the left focus, i.e., $\vec{R}_0 = -\vec{R}$ in the notations of Fig. 1.

Consider now an STM tip placed directly above the surface point \vec{r} . If the tip couples predominantly to the underlying surface-state electrons at \vec{r} , then the differential conductance for the current through the STM tip measures, up to thermal broadening, the local surface-electron density of states at point \vec{r} , $\rho(\vec{r}, \epsilon)$. For an isolated Co impurity, $\rho(\vec{r}, \epsilon)$ depends on the Kondo scattering from the impurity as described, e.g., in Ref. [6]. For the multiple-impurity configuration considered here there are two main modifications: (i) There are multiple scattering off the different Co adatoms; (ii) Intersite correlations alter the Kondo scattering off each Co adatom. Due to the relatively large distance between Co atoms ($\sim 10\text{\AA}$ for neighboring atoms on the ellipse perimeter), we expect the latter effect to be small, and therefore neglect it hereafter.

Since we are mostly interested in the effect of the Co atom placed inside the ellipse, we distinguish it from the other Co atoms on the perimeter of the ellipse. Neglecting intersite correlations, $\rho(\vec{r}, \epsilon)$ takes the form $\rho(\vec{r}, \epsilon) = \bar{\rho}(\vec{r}, \epsilon) + \delta\rho(\vec{r}, \epsilon)$, where

$$\bar{\rho}(\vec{r}, \epsilon) = -\frac{1}{\pi} \text{Im}\{G(\vec{r}, \vec{r}; \epsilon)\} \quad (1)$$

is the density of states of an empty ellipse (i.e., in the absence of the inner adatom), and

$$\delta\rho(\vec{r}, \epsilon) = -\frac{1}{\pi} \text{Im}\{t_s^2 G(\vec{r}, \vec{R}_0; \epsilon) G_d(\epsilon) G(\vec{R}_0, \vec{r}; \epsilon)\} \quad (2)$$

is the additional contribution due to the extra Co atom at \vec{R}_0 . Here $G(\vec{r}, \vec{r}'; \epsilon)$ is the retarded Green function of the surface electrons for an empty ellipse, and $G_d(\epsilon)$ is the fully dressed retarded Green function of the d electrons of the inner adatom. Note that in writing Eq. (2) we have assumed that the three-dimensional propagation of bulk electrons between different Co sites on the surface is small compared to the two-dimensional propagation of the surface electrons. This assumption is quite reasonable considering that the three-dimensional propagation near the surface decays as $1/r^2$, compared to $1/\sqrt{r}$ for the two-dimensional surface propagation [7].

Experimentally, $\delta\rho(\vec{r}, \epsilon)$ is extracted by first measuring the local density of states of the empty ellipse, and then subtracting it from the measured density of states with the extra Co atom. To compute $\delta\rho(\vec{r}, \epsilon)$, one needs to evaluate $G(\vec{r}, \vec{r}'; \epsilon)$, which is our next goal. To this end,

we introduce the $N \times N$ matrix $g_{ij} \equiv (1 - \delta_{ij})G_0(\vec{R}_i, \vec{R}_j)$, along with the two vector quantities, $v_i = G_0(\vec{r}, \vec{R}_i)$ and $u_i = G_0(\vec{R}_i, \vec{r}')$. Here $G_0(\vec{r}, \vec{r}')$ is the free surface Green function without the corral, and i and j run over $1, \dots, N$. Using these quantities, $G(\vec{r}, \vec{r}'; \epsilon)$ is compactly expressed as

$$G(\vec{r}, \vec{r}'; \epsilon) = G_0(\vec{r}, \vec{r}') + \sum_{i,j=1}^N v_i \left[\frac{1}{1 - Tg} T \right]_{ij} u_j, \quad (3)$$

where $T(\epsilon) = t_s^2 G_d(\epsilon)$ is the surface-to-surface component of the conduction-electron scattering T -matrix at each Co site. Again, Eq. (3) omits the intersite correlations and the bulk propagation between different Co sites. Finally, for temperatures and energies below the Kondo temperature, the Kondo part of $G_d(\epsilon)$ may be well approximated [8] by the Lorentzian form $Z_K / (\epsilon - \epsilon_F + iT_K)$, where T_K is the Kondo temperature, ϵ_F is the Fermi energy, and

$$Z_K = \frac{T_K}{\pi\rho_s t_s^2 + \pi\rho_b t_b^2} \quad (4)$$

is the corresponding weight. Here ρ_s and ρ_b are the surface and bulk density of states at the Fermi level.

A key parameter that enters the quantum mirage is the ratio of scattering rates

$$t = \frac{\pi\rho_s t_s^2}{\pi\rho_s t_s^2 + \pi\rho_b t_b^2}. \quad (5)$$

Physically, t represents the probability that a surface-state electron impinging on a Co adatom will be scattered to a surface-state electron rather than a bulk electron. Hence t is a measure of the in-elasticity of the scattering of surface waves from the Co impurities. In the theory of Heller *et al.* [9] for the standing waves formed in a quantum corral, t is found to be $1/2$. Hereafter we shall use the same value for t .

In Fig. 2 we depict $\delta\rho(\vec{r}, \epsilon_F)$ for various configurations of the Co atoms, as measured by Manoharan *et al.* [1]. The upper panels correspond to an ellipse with eccentricity $\mathcal{E} = 0.786$ and 34 adatoms (ellipse **b** of Ref. [1]), while the lower panels correspond to an ellipse with eccentricity $\mathcal{E} = 0.5$ and 36 adatoms (ellipse **a** in Ref. [1]). The quantum mirage is clearly seen in each of the left two panels, where an additional adatom has been placed at the left focus of the ellipse. For both ellipses, there is a strong signal in the tunneling density of states right above the right focus, in accordance with the experimental data. By contrast, the quantum mirage disappears when the additional adatom is placed off the focus, as shown in the right two panels. These results are in good agreement with the experimental measurements, reproducing even fine details of the experimental patterns.

The results of Fig. 2 were obtained from Eqs. (2) and (3), by setting $t = 1/2$ and approximating G_0 with the free two-dimensional Green function:

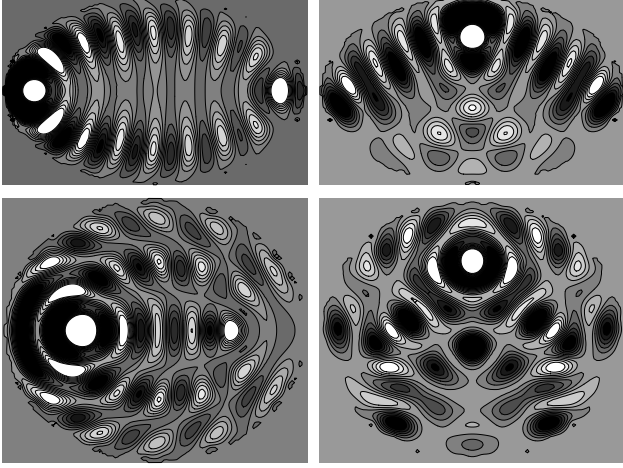


FIG. 2. Contour plot of $\delta\rho(\vec{r}, \epsilon_F)$ at the Fermi level assuming $t = 1/2$. The upper panels correspond to an ellipse with eccentricity $\mathcal{E} = 0.786$ and 34 adatoms, while the lower panels to an ellipse with $\mathcal{E} = 0.5$ and 36 adatoms. For both ellipses, a strong signal appears at the right focus of the ellipse when an additional adatom has been placed at the left focus. This quantum mirage disappears when the additional adatom is placed off the focus, as shown in the right two panels.

$$G_0(\vec{r}, \vec{r}') = -i\pi\rho_s H_0^{(1)}(k|\vec{r} - \vec{r}'|). \quad (6)$$

Here k is the wave number, and $H_0^{(1)}(x)$ is the Hankel function of zeroth order, which for $x \gg 1$ takes the asymptotic form

$$H_0^{(1)}(x) \simeq \sqrt{\frac{2}{\pi x}} \exp\left(ix - i\frac{\pi}{4}\right). \quad (7)$$

The good agreement between our calculations with $t = 1/2$ and the experimental data indicates that the number of scattering events that a particle undergoes before leaving the surface bounded by the ellipse is small. This suggests the possibility of calculating the quantum mirage at the right focus at the Fermi level, $\delta\rho(\vec{R}, \epsilon_F)$, using perturbation theory in t . Thus, to linear order in t , the Green function between the left and the right foci is given by

$$G(-\vec{R}, \vec{R}; \epsilon_F) \simeq G_0(-\vec{R}, \vec{R}) + G_1(-\vec{R}, \vec{R}) + \dots, \quad (8)$$

where

$$G_0(-\vec{R}, \vec{R}) \simeq -i\rho_s \sqrt{\frac{\pi}{\mathcal{E}k_F a}} e^{i2\mathcal{E}k_F a - i\frac{\pi}{4}} \quad (9)$$

is the contribution of the direct path connecting the two foci (illustrated by the dashed line in Fig. 1), and

$$G_1(-\vec{R}, \vec{R}) = \frac{t}{i\pi\rho_s} \sum_{j=1}^N G_0(-\vec{R}, \vec{R}_j) G_0(\vec{R}_j, \vec{R}) \quad (10)$$

comes from all trajectories which scatter from a single Co adatom on the ellipse perimeter (solid lines in Fig. 1).

Conventionally, the second term G_1 is smaller than G_0 for several reasons. First, each scattering event is inelastic, and therefore introduces a reduction factor of t . Second, the scattered orbits are longer. Third, the various orbits have generally different lengths, and therefore their corresponding phases add up incoherently. The situation is quite different in the present case. Due to the defining property of the ellipse, the length of all scattered orbits between the two foci is precisely the same, and hence their contributions add up coherently. Consequently, the second term in Eq. (8) takes the form

$$G_1(-\vec{R}, \vec{R}) \simeq i\rho_s \sum_{j=1}^N \frac{2t}{k_F \sqrt{\xi_{1,j} \xi_{2,j}}} e^{i2k_F a - i\frac{\pi}{2}}, \quad (11)$$

where $2a$ is the length of each orbit, and $\xi_{1,j}$ and $\xi_{2,j}$ are the distances between the impurity at \vec{R}_j and the right and left foci, respectively (see Fig. 1). Finally, we approximate the sum in Eq. (11) by an integral:

$$\sum_{j=1}^N \frac{1}{\sqrt{\xi_{1,j} \xi_{2,j}}} \simeq \frac{1}{d} \oint ds \frac{1}{\sqrt{\xi_1(s) \xi_2(s)}}, \quad (12)$$

where s denotes the coordinate along the ellipse contour, and d is the mean distance between adjacent adatoms. The result of the integral is independent of the eccentricity of the ellipse, and is simply 2π . Thus, the contribution of orbits scattered from a single perimeter adatom is

$$G_1(-\vec{R}, \vec{R}) \simeq \rho_s \frac{4\pi t}{k_F d} e^{i2k_F a}. \quad (13)$$

Comparing $G_0(-\vec{R}, \vec{R})$ and $G_1(-\vec{R}, \vec{R})$ at the Fermi energy, one sees that the leading contribution to the quantum mirage comes from G_1 [10], provided

$$\frac{d}{\mathcal{E}a} \ll \frac{16\pi t^2}{k_F d}. \quad (14)$$

Substituting the experimental parameters, $d \simeq 10\text{\AA}$, $a \simeq 70\text{\AA}$, and $k_F \simeq 1/4.75\text{\AA}^{-1}$, and setting $t = 1/2$, it is straightforward to verify that Eq. (14) holds for all ellipses with eccentricity $0.05 < \mathcal{E} < 1$. Furthermore, Eq. (14) is always satisfied for sufficiently large ellipses, provided the mean distance between adjacent adatoms is kept fixed ($a \gg d$).

Neglecting the contribution of the direct path, $G_0(-\vec{R}, \vec{R})$, and using Eqs. (2) and (13) with $\vec{r} = \vec{R}$, the resulting local density of states at the Fermi energy takes the form

$$\delta\rho(\vec{R}, \epsilon_F) \simeq \rho_s \frac{16t^3}{(k_F d)^2} \cos(4k_F a). \quad (15)$$

The main feature of the above result is the robustness of the quantum mirage: As long as condition (14) is satisfied, the amplitude of the mirage is independent of the

size of the ellipse, a , and its eccentricity, \mathcal{E} . Rather, the amplitude is determined by t , which characterizes the inelasticity of the scattering of surface waves from adatoms, and the dimensionless mean distance between adjacent adatoms along the ellipse, $k_F d$. The oscillations of the mirage as function of a are indeed periodic with a period of $\lambda_F/4$, as seen experimentally [1].

Next we consider the effect of a weak uniform magnetic field, B , applied perpendicular to the surface. As shown below, the quantum mirage experiences a distinctive oscillatory behavior as a function of the magnetic field, which depends on the size and the shape of the ellipse. Here we assume that the ellipse is sufficiently large and that the magnetic field is sufficiently weak so that (i) Zeeman splitting of the Kondo resonance can be neglected, and (ii) the cyclotron radius of the conduction electrons is much larger than the ellipse size.

Under these circumstances, the main effect of the magnetic field is to introduce an additional Aharonov-Bohm phase to the contribution of each path. This phase is the magnetic flux encircled by the orbit, measured in units of the quantum flux, $\phi_0 = hc/e$. Here h is Planck's constant, c is the velocity of light, and e is the electron charge. To compute $G_1(-\vec{R}, \vec{R})$ we fix the gauge by calculating the flux encircled by the path which goes from \vec{R} to \vec{R}_j , to $-\vec{R}$, and then back to \vec{R} along the semimajor axis of the ellipse. Accordingly, the sum of Eq. (11) is modified to $\sum_j (\xi_{1,j} \xi_{2,j})^{-1/2} e^{i2\pi\varphi_j/\phi_0}$, where φ_j is the flux of each trajectory. Using the continuum approximation of Eq. (12) this sum gives $2\pi J_0(2\mathcal{E}AB/\phi_0)$, where $J_0(x)$ is the Bessel function of zeroth order, and $\mathcal{A} = \pi a^2 \sqrt{1 - \mathcal{E}^2}$ is the area of the ellipse. The quantum mirage is, thus, modified according to

$$\delta\rho(B) \simeq \delta\rho(0) J_0^2 \left(2\mathcal{E} \frac{AB}{\phi_0} \right), \quad (16)$$

where $\delta\rho(0)$ is the zero-field result of Eq. (15). Note that, for a given a , the sensitivity to a magnetic field is largest for $\mathcal{E} = 1/\sqrt{2}$.

Finally, we discuss the role of imperfections in the ellipse. Clearly, a combined effect of many coherent trajectories is very sensitive to imperfections and dephasing. At 4K, dephasing effects due to electron-electron and electron-phonon interactions are negligible over distances of the order of hundreds of angstroms. In what follows we show that effect of imperfections is small too.

The main source of imperfections in the ellipse comes from the position of the adatoms forming the ellipse. These are constrained to sit on a triangular lattice imposed by the underlying Cu(111) surface. Consequently, the lengths of the orbits contributing to $\delta\rho$ are not those of an ideal ellipse. To estimate the effect of the deviations, we consider a random distribution of the trajectory lengths, and average over the distribution. We first notice that each contribution to $\delta\rho$ is composed of 4 segments:

ξ_1 , ξ_2 , ξ_3 , and ξ_4 , as illustrated in Fig. 1. Each of these segments is regarded as an independent random variable uniformly distributed in the range $(\xi - b/2, \xi + b/2)$, where ξ is the exact distance from the focus to the ellipse boundary, and b is the triangular lattice spacing. The total length $\eta = \sum_{n=1,4} \xi_n$ is, therefore, approximately a Gaussian random variable with mean $4a$ and variance $b^2/3$. Averaging the cosine term in Eq. (15), $\langle \cos(k_F \eta) \rangle$, the disorder-averaged value of the quantum mirage is reduced by a factor of approximately $Q = \exp(-k_F^2 b^2/6)$. Substituting the experimental values $k_F = 1/4.75\text{\AA}^{-1}$ and $b = 2.55\text{\AA}$, one finds $Q \approx 0.95$, meaning that the effect of imperfections is negligible.

In conclusion, in this Letter we have studied the phenomenon of quantum mirage, and clarified its relation to the classical orbits of a particle in an ellipse. Our theory also predicts a distinctive behavior of the quantum mirage in the presence of a perpendicular magnetic field, which could be tested experimentally. Finally our approach clearly shows that the phenomenon of quantum mirage is not unique for magnetic adatoms. It will also appear for nonmagnetic atoms (on the ellipse perimeter or at its focus) with strong scattering, e.g. adatoms with resonant tunneling states at the Fermi level.

A.S. is grateful to Hari Manoharan for useful discussions. This research was supported by the Israel science foundation founded by The Israel Academy of Science and Humanities, and by Grant No. 9800065 from the USA-Israel Binational Science Foundation (BSF).

-
- [1] H. C. Manoharan, C. P. Lutz, and D. M. Eigler, *Nature* **403** 512 (2000).
 - [2] J. Li, W.-D. Schneider, R. Berndt, and B. Delley, *Phys. Rev. Lett.* **80**, 2893 (1998).
 - [3] V. Madhavan, W. Chen, T. Jamneala, M. F. Crommie, and N. S. Wingreen, *Science* **280**, 567 (1998).
 - [4] For a microscopic derivation of a nondegenerate Anderson model description of a Co adatom on Au(111), see O. Újsághy, J. Kroha, L. Szunyogh, A. Zawadowski, *Phys. Rev. Lett.* **85**, 3690 (2000).
 - [5] P. W. Anderson, *Phys. Rev.* **124**, 41 (1961).
 - [6] A. Schiller and S. Hershfield, *Phys. Rev. B* **61**, 9036 (2000).
 - [7] Conventionally, free 3D propagation over a distance of r decays as $1/r$. Near the surface, though, the power law changes to $1/r^2$, due to the surface boundary condition (corresponding to an image charge).
 - [8] See, e.g., A. Hewson, *"The Kondo Problem to Heavy Fermions,"* (Cambridge Press, Cambridge, 1993).
 - [9] E. J. Heller, M. F. Crommie, L. P. Lutz, and D. M. Eigler, *Nature* **369** 464 (1994).
 - [10] One may be concerned about higher order terms, such as G_2 , G_3 , etc. These, however, are small, as they represent mainly non-classical paths, whose contributions add up incoherently.